Published online 1 June 2016

Nucleic Acids Research, 2016, Vol. 44, No. 16 ***7911–7921***
doi: 10.1093/nar/gkw507

The catalytic efficiency of yeast ribonuclease III depends on substrate specific product release rate

Marc-Andre Comeau[1], Daniel A. Lafontaine[1,*] and Sherif Abou Elela[2,*]

[1]Département de biologie, Faculté de science, Université de Sherbrooke, Sherbrooke, Québec J1E 2R1, Canada and [2]Département de microbiologie et d'infectiologie, Faculté de médecine et des sciences de la santé, Université de Sherbrooke, Pavillon de recherche appliquée sur le cancer, Sherbrooke, Québec J1E 4K8, Canada

Received March 07, 2016; Revised May 24, 2016; Accepted May 25, 2016

ABSTRACT

Members of the ribonuclease III (RNase III) family regulate gene expression by triggering the degradation of double stranded RNA (dsRNA). Hundreds of RNase III cleavage targets have been identified and their impact on RNA maturation and stability is now established. However, the mechanism defining substrates' reactivity remains unclear. In this study, we developed a real-time FRET assay for the detection of dsRNA degradation by yeast RNase III (Rnt1p) and characterized the kinetic bottlenecks controlling the reactivity of different substrates. Surprisingly, the results indicate that Rnt1p cleavage reaction is not only limited by the rate of catalysis but can also depend on base-pairing of product termini. Cleavage products terminating with paired nucleotides, like the degradation signals found in coding mRNA sequence, were less reactive and more prone to inhibition than products having unpaired nucleotides found in non-coding RNA substrates. Mutational analysis of U5 snRNA and Mig2 mRNA confirms the pairing of the cleavage site as a major determinant for the difference between cleavage rates of coding and non-coding RNA. Together the data indicate that the base-pairing of Rnt1p substrates encodes reactivity determinants that permit both constitutive processing of non-coding RNA while limiting the rate of mRNA degradation.

INTRODUCTION

RNase III is a ubiquitous dsRNA processing enzyme found in all kingdoms of life except archaebacteria (1,2). Members of the RNase III family are defined by the presence of the catalytic (RIIID) (3,4) and the dsRNA-binding (dsRBD) (5) domains, which were first identified in bacteria (6). In the yeast *Saccharomyces cerevisiae*, Rnt1p is an RNase III ortholog involved in the degradation of unspliced mRNA (7,8), conditional mRNA decay (9–11) and the processing of many non-coding RNAs such as small nuclear RNAs (snRNAs) (12–16), pre-rRNAs (17) and small nucleolar RNAs (snoRNAs) (8). In the case of non-coding RNA like the U5 snRNA a robust and constitutive reactivity is required to ensure the maturation of the hundreds of RNA molecules required for the spliceosome (13). In contrast, the degradation of mRNA produced by scarcely expressed genes like the glucose-dependent gene *MIG2* or the telomerase subunit gene *EST1* requires moderate substrate reactivity that permits controlled and often conditional RNA cleavage (9,18). Indeed, insertion of different Rnt1p cleavage signals in a heterologous reporter indicated that substrates originating from non-coding RNA are much more reactive than those originating from mRNA (19). However, the mechanism generating this differential substrate reactivity remains unclear.

Rnt1p recognizes RNA substrates with stem–loop structures containing NGNN tetraloops (G2-tetraloop) (20). The enzyme identifies its substrate by interacting with multiple nucleotides within the loop and its neighboring stem structure (21). In general, a G2-tetraloop with a minimum of three base pairs (22) is required for two specific cleavages to occur at 14 and 16 nucleotides from the terminal loop (Figure 1A). The typical cleavage reaction produces a 34-nucleotide stem–loop structure terminating with a 3′ overhang and two RNA fragments corresponding to the sequences upstream and downstream of the cleavage site (Figure 1A) (23,24). The tetraloop structure is essential for the recognition and cleavage of the G2 substrates, while the sequence of the stem controls the substrate turnover rate (22,24) by an as yet unidentified mechanism.

Recent work has indicated that the enzyme uses a special clamp-like structure at the end of the dsRBD domain to specifically recognize the conserved guanine in the second position of the loop (22). The structure of the catalytic complex is assembled through interaction with the substrate via five RNA binding motifs (RBMs). As indicated in Figure 1A, RBM0, which contains the clamp structure, interacts

*To whom correspondence should be addressed. Tel: +1 819 821 8000 (Ext. 75275); Fax: +1 819 820 6831; Email: Sherif.Abou.Elela@USherbrooke.ca
Correspondence may also be addressed to Daniel A. Lafontaine. Tel: +1 819 821 8000 (Ext. 65011); Email: Daniel.Lafontaine@USherbrooke.ca

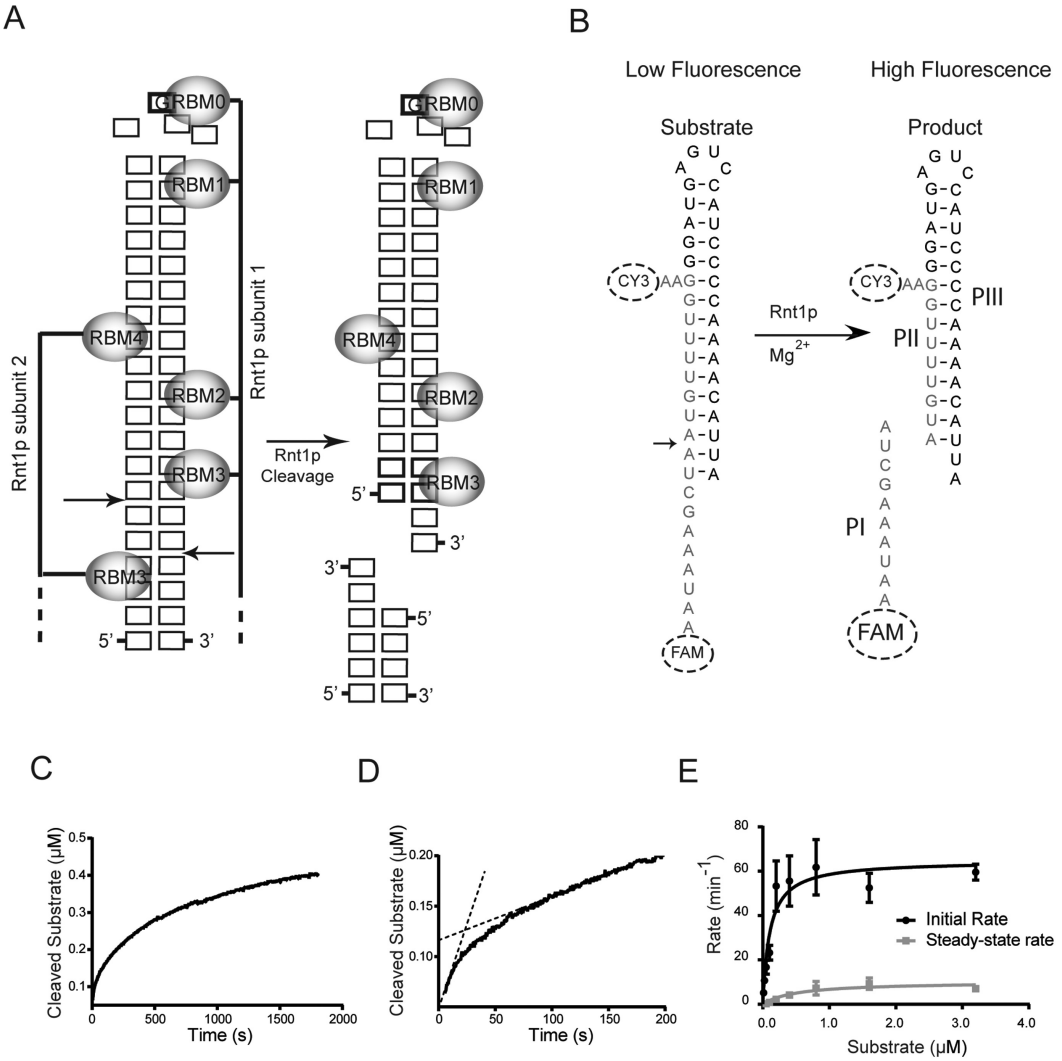

Figure 1. Continuous fluorescence assay of Rnt1p cleavage reveals rapid pre-steady state kinetics. (**A**) Mechanism of Rnt1p binding and cleavage. The Rnt1p G2-substrate is shown in the form of a stem sloop structure. The nucleotides are shown as boxes and the position of the conserved guanine is indicated by a G. The canonical structure of Rnt1p substrates is outlined and its RNA binding motifs (RBM) are indicated as gray circles. In this model, cleavage eliminates the interaction between Rnt1p and the RNA sequence downstream of the cleavage site, which permits the enzyme to discriminate between the substrates and its products. (**B**) Strategy for detecting Rnt1p-mediated cleavage in real-time. Schematic representation of the bipartite substrates used for the fluorescence cleavage assay. The substrate is created by annealing an RNA strand (shown in grey) labeled with fluorescent dyes (6-FAM and CY3) to the G2–stem–loop (shown in black). Rnt1p cleavage releases the 6-FAM dye from the CY3 quencher, which permits the detection of the enzyme catalytic activity in real-time. **C**) Fluorescence profile of Rnt1p cleavage. The substrate shown in (B) (0.8 μM) was incubated with the enzyme under physiological salt conditions (150 mM) and the change in fluorescence was continuously monitored for 30 min. (**D**) Analysis of Rnt1p early cleavage kinetics reveals two distinct catalytic rates. The profile of the first 200 s of the cleavage reaction shown in (C) was expanded to reveal the biphasic nature of Rnt1p cleavage kinetics. The dashed line indicates the extrapolated trajectory of catalysis in each phase. (**E**) Comparison between the kinetic profiles of initial and steady-state rates of catalysis. The Michaelis-Menten graph was generated based on the initial and steady-state rates for concentrations of substrate from 50 nM to 1600 nM. The data shown are the average of at least three independent assays and the standard deviations are shown in the form of error bars.

with the G2-loop during the initial steps of the complex formation. In addition, Rnt1p employs RBM1 to interact with the nucleotides adjacent to the tetraloop, RBM2 and RBM4 interact with the RNA of the stem and RBM3 contacts the nucleotides surrounding the cleavage site (22). Most binding sites are maintained with the cleavage product except RBM3, which binds less stably after catalysis (Figure 1A).

RNase III binds its substrates in the absence of divalent metal ions (25) but requires Mg^{2+} for cleavage. The divalent metal ions position and activate water molecules, located near the cleavage site, to induce catalysis (2). The rate of the hydrolytic step is dependent on the metal ion's pK_a (26). Hydrolysis leads to the generation of products terminating with 3′-hydroxyl and 5′-phosphomonoester groups (22,27–29). Chemical substitution near Rnt1p substrate's scissile bonds indicated that it is the position of the phosphodiester backbone relative to the enzyme rather than the 2′-OH groups that is critical for cleavage by Rnt1p (29).

Biochemical and structural analysis of Rnt1p suggest that RNA recognition is initiated by a base-specific interaction between the G-clamp (RBM0) and the second nucleotide of the loop (22). This interaction is formed to

strengthen the complex and to prevent catalytic domain slippage along the RNA helix (22). If this initial recognition is successful, the substrate is loaded into the nuclease domain through direct interactions with the Rnt1p RBM1–4 and then cleaved at a fixed distance from the loop (22). The process leading to product release and its impact on the turnover rate of Rnt1p, and of RNase III enzymes in general, is not fully understood. Comparison between different Rnt1p cleavage signals indicates wide variation in substrate turnover rate. In general, rRNA and snoRNA substrates are much more efficiently cleaved, *in vivo* and *in vitro,* by Rnt1p than mRNA substrates (e.g. Mig2 and Fit2). However, the molecular mechanisms controlling the reactivity of different Rnt1p substrates remain unclear. Despite decades of biochemical and genetic analyses of RNase III orthologs, we still do not know what determines the enzyme turnover rate.

To understand the mechanisms controlling the reactivity of Rnt1p substrates, we developed a fluorescence assay to monitor the real time kinetics of Rnt1p cleavage activity and to identify the critical steps in the enzymatic reaction. Our results indicate that the substrate reactivity is defined by the rate of product release and suggest that the base-pairing surrounding the cleavage site determines the substrate turnover rate. Products generated from the cleavage of efficiently processed substrates, like U5 snRNA, have low affinity for the enzyme and thus have high dissociation rates. In contrast, products generated from inefficiently cleaved substrates, like Mig2 mRNA, have high affinity and slow dissociation rates. Comparison of the products generated by substrates with different cleavage rates indicates that base pairing upstream of the cleavage site reduces the rate of product release and decreases turnover. Consistently, disruption of base pairing near the cleavage site increased the turnover rate by promoting product dissociation. Together, our data reveals that the reactivity of yeast RNase III substrates depends on the base-pairing surrounding the cleavage. This rate limiting step has likely been exploited by evolution to meet the demand of genes with different functions and expression levels.

MATERIALS AND METHODS

Real-time analysis of Rnt1p cleavage kinetics

Recombinant enzyme was expressed and purified as previously described (30). Synthetic RNA with 6-FAM at the 5′ end and an amino linker at the 3′ end was obtained from Integrated DNA Technologies (IDT – Coralville, Iowa). Labeling of the RNA target portion (Figure 1B) was completed by incubating 150 μg of RNA with 25 μg of Cy3 dye overnight in 0.1 M sodium tetraborate at pH 8.5. The labeled RNA was purified using 20% PAGE and extracted via electro-elution (30). The bipartite RNA substrate was reconstituted by annealing 50–1600 nM of a 1:8 mix of labeled to unlabeled target strands to an equal amount of guide RNA as previously described (21). Cleavage reactions were performed at 30°C using 7.5 nM of purified Rnt1p in a reaction buffer containing 30 mM Tris–HCl, pH 7.5, 5 mM spermidine, 0.1 mM DTT, 0.1 mM EDTA and 10 mM $MgCl_2$. The monovalent salt concentration was 150 mM KCl unless noted otherwise. RNA cleavage was monitored in real-time using a Quanta Master system (PTI, London, Ontario, Canada) or Flex Station (Molecular Device, Sunnyvale, CA, USA) by exciting the fluorophores at 490 nm and monitoring the fluorescence emission at 520 nm. The cleavage reaction was stopped by adding a solution containing 75 mM EDTA and 85% formamide, and the cleavage products were separated using 20% PAGE. The fluorescent cleavage products were visualized on a Typhoon Trio (GE Healthcare Life Sciences, Burnaby, BC, Canada) with the fluorescein channel. The cleavage rates of cleavage reactions were either determined by linear regression or, in case of biphasic reaction, with non-linear fitting of an exponential burst phase followed by a linear steady-state phase over the first minute of reaction according to the following model: $Y = Y_{fast}(1 - e^{-k_{fast}*t}) + k_{slow} * t$. The kinetic parameters were calculated using a standard Michaelis–Menten model. The product inhibition assays were conducted using 800 nM of synthetic RNA products added to the reaction.

In vitro cleavage assay

Xrn1p protein was purified as previously reported (31). Standard gel-based Rnt1p cleavage assays were performed using 30 nM Rnt1p and trace amounts of internally radiolabeled RNA already mixed with 1600 nM unlabeled RNA in a standard reaction buffer (30 mM Tris–HCl, pH 7.5, 5 mM spermidine, 0.1 mM DTT, 0.1 mM EDTA, 10 mM $MgCl_2$ and 150 mM KCl). The effect of product inhibition on Rnt1p cleavage was tested by including 74 nM of purified Xrn1p to the standard Rnt1p cleavage assay. The specificity of the Xrn1p effects was tested by incubating Xrn1p with the RNA in the absence of Rnt1p. An equal amount of inactive (boiled) Xrn1p was added in Rnt1p cleavage assays. Product titration reactions were performed using trace amounts of 5' radiolabeled RNA, already mixed with 1600 nM of unlabeled RNA, in the presence of 0–3.200 μM synthetic Rnt1p products. All *in vitro* assays were carried out for 10 min, stopped by the addition of 85% formamide (Bioshop Canada, Burlington, Ontario, Canada) containing 75 mM EDTA, pH 8.0, and resolved by 20% PAGE. The cleavage products were visualized using autoradiography as previously described (30).

Surface plasmon resonance binding assay

RNA binding to purified Rnt1p was monitored using a Biacore T200 system (GE Healthcare Life Sciences, Burnaby, BC, Canada). The assays were carried out in binding buffer containing 30 mM HEPES, pH 7.5, 150 mM KCl and 10 nM EDTA. The effect of magnesium ions was tested by adding 10 mM $MgCl_2$ to the reaction. His-tagged Rnt1p was immobilized on Ni-NTA chip via the His-tag prior to RNA injection. The surface was washed with 350 mM EDTA and 0.1% SDS between each sample injection. Binding was calculated relative to the amount of protein bound to the chip for each RNA concentration to generate resonance unit change (RU) over the theoretical maximal RU (Rmax) values. RNA concentrations ranging from 50 to 1600 nM were used for each binding assay. On (association) and off (dissociation) rates were calculated with Biacore T200 software using a single binding site model on all curves.

RESULTS

Design of a fluorescent reporter of Rnt1p cleavage activity

We have previously shown that Rnt1p can use short RNA transcripts as guides for the cleavage of RNA targets *in trans* (21,32). In this assay we annealed guide and target RNAs to generate highly reactive bipartite substrates that undergo RNA processing *in vivo* (32) and mimic the cleavage kinetics of natural substrates *in vitro* (21). In this study, we further developed this bipartite system by generating a fluorescent reporter for real time observation of Rnt1p cleavage kinetics. The reporter was generated by annealing an unlabeled guide RNA to a target strand labeled with both fluorescent donor (6-FAM) and acceptor (Cy3) dyes (Figure 1B). Cleavage of the reporter generates 3 RNA fragments (Figure 1B), a short single-stranded 5′ fragment (PI), an intermediate single-stranded fragment (PII) and a 3′ end stem–loop structure (PIII). PII and PIII retain significant sequence complementarity and are expected to remain in a complex after cleavage thus generating only one product capable of binding to Rnt1p (32). Indeed, the PII/PIII mixture and its associated bipartite substrate generate similar circular dichroism spectra under cleavage conditions confirming similar overall helicity of these two structures (Supplementary Figure S1F). The intact RNA target is expected to generate low signal due to the fluorescence resonance energy transfer (FRET) occurring between the fluorophores (33). However, once the RNA substrate is cleaved, the fluorescence signal is expected to increase as no more FRET occurs between 6-FAM and the Cy3 quencher. To test this reporter, we first monitored Rnt1p cleavage under multiple turnover conditions with an excess of substrate. The cleavage reaction was performed at physiological monovalent salt concentration (i.e. 150 mM KCl), which provides optimal specificity and turnover rate (30). The cleavage reaction was initiated by adding 10 mM $MgCl_2$ to a reaction buffer containing Rnt1p and the fluorescent substrate (see Material and Methods). As indicated in Supplementary Figure S1A, a strong increase in fluorescence was detected after initiating the reaction and the signal level was directly related to the proportion of cleaved substrates (Supplementary Figure S1B). Incubating the reporter substrate with increasing amounts of Rnt1p in the absence of $MgCl_2$, which permits binding but not cleavage of the RNA (25), did not affect the fluorescence signal (Supplementary Figure S1C). This indicates that cleavage is required for the generation of the fluorescence signal. Comparison between the fluorescence and conventional gel-based cleavage assay indicated that both methods generate similar cleavage kinetics, both as a function of time (Supplementary Figure S1D) and of optimum substrate concentrations (Supplementary Figure S1E). Together these experiments demonstrate the utility and precision of our bipartite fluorescent substrate as a reporter of Rnt1p catalytic activity.

Monitoring Rnt1p cleavage kinetics in real time

To determine the real time kinetics of Rnt1p-mediated cleavage, we plotted product accumulation over time (Figure 1C). The resulting curve suggests the presence of a fast initial phase (burst phase) followed by a slower phase consistent with product inhibition. Indeed, closer inspection of the first 200 s of the reaction confirmed the presence of this two phases (Figure 1D). Measuring the cleavage rate over a range of substrate concentrations yielded a catalytic rate constant (k_{cat}) of $64.7 \pm 5.8\ min^{-1}$ for the burst phase, which exhibited a standard hyperbolic Michaelis-Menten curve, and $10.1 \pm 1.2\ min^{-1}$ for the later phase of the reaction (Figure 1E), which resembles the so called steady state kinetics of the in gel cleavage assays and there {Lamontagne, 2001 #472}. We also observed that the Km is increased from $0.11 \pm 0.04\ \mu M$ for the burst phase to $0.51 \pm 0.17\ \mu M$ in the later phase, which probably results from the accumulation of the product and change in the substrate concentration (Supplementary Figure S2B and Table S1). To evaluate the contribution of binding affinity to the decreased rate of the steady-state phase, we monitored the cleavage kinetics at increasing concentrations of monovalent salts, which weakens the interaction of Rnt1p with its substrates (25). As predicted, increasing the salt concentration to 500 mM disrupted the biphasic progression of the cleavage reaction (Supplementary Figure S1E). This suggests that the slower rate of the steady-state is not due to a decrease in the complex stability but instead points at steps after the initial recognition and binding of the substrates.

The cleavage products determine the turnover rate of Rnt1p

To examine the contribution of cleavage-product dissociation to Rnt1p kinetics, we synthesized RNA molecules that mimic the stem–loop structure produced by Rnt1p cleavage (Figure 2A), and monitored their impact on turnover. As shown in Figure 2B, the addition of products to the cleavage reaction reduced the initial rate of catalysis and eliminated the burst phase (Figure 2B). When analyzing the product inhibitory effect at various substrate concentrations, we found that the presence of $0.8\ \mu M$ products reduced the value of the initial phase k_{cat} by 5-fold ($12 \pm 5\ min^{-1}$) (Figure 2C and Supplementary Table S1). The reduction of Rnt1p activity by the product is impaired when the reaction is carried out with a buffer containing 500 mM KCl, which reduces the stability of Rnt1p/RNA complex (Supplementary Figures S2C and S2D). This indicates that the capacity of the product to inhibit the cleavage reaction depends on its capacity to form a stable complex with the enzyme and suggest that the substrate binding to the enzyme is more stable than its product.

Given that Rnt1p catalytic activity appears to be inhibited by the accumulation of cleavage products, we reasoned that the elimination of these products should increase the cleavage rate. To test this hypothesis we monitored the cleavage reaction after the addition of a recombinant version of the 5′-3′ exoribonuclease Xrn1p (34), which was previously shown to degrade the 3′ product of Rnt1p *in vivo* and *in vitro* without affecting the substrates (10,19). In the case of the fluorescent reporter, Xrn1p will degrade the intermediate cleavage product of Rnt1p (PII, Figure 1A), which possesses a 5′ monophosphate, and leave behind a short stem–loop structure and single-stranded fragments. Degradation of the intermediate products (PII) eliminates all base pairing near the cleavage site and increases the difference between the structure of the substrate and its product. As pre-

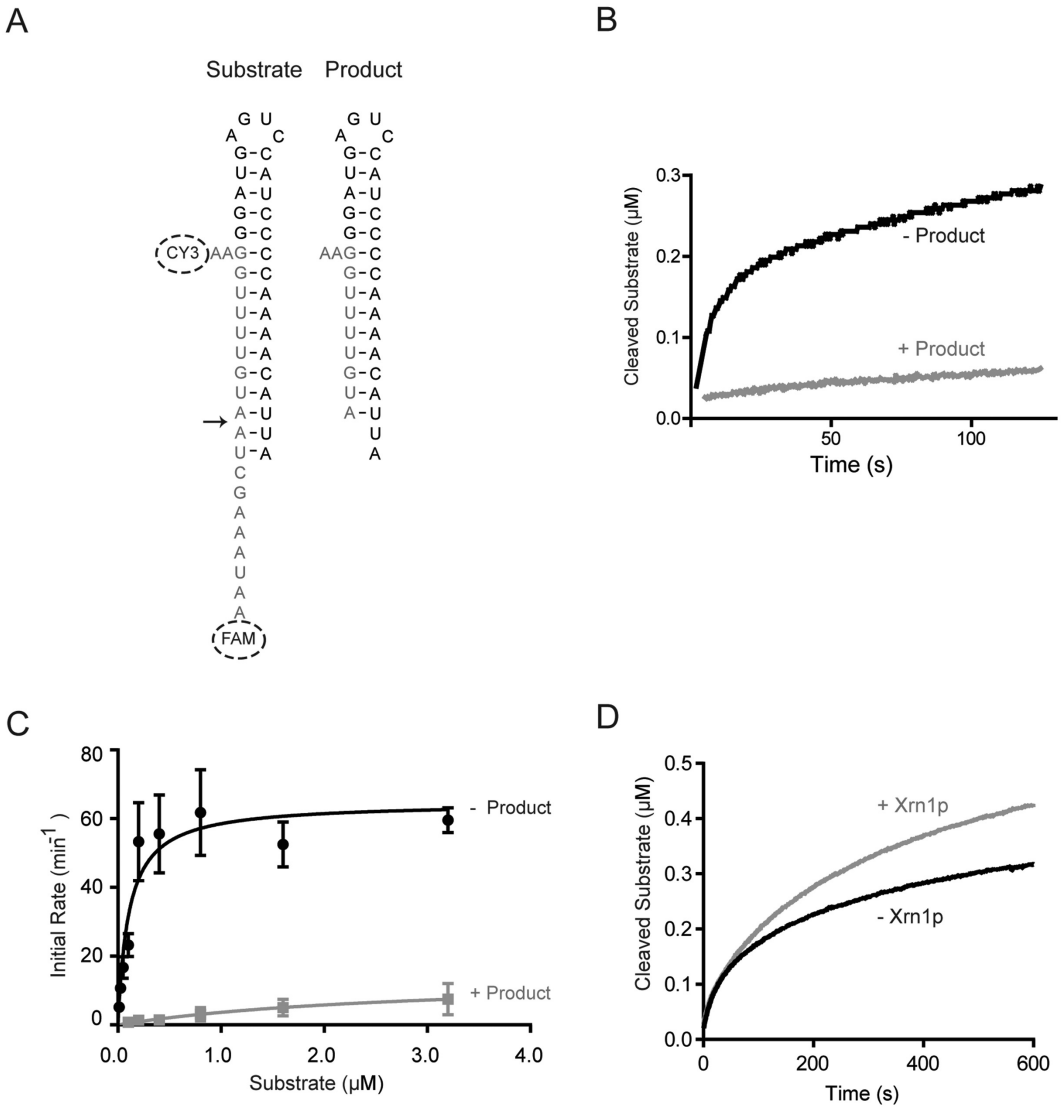

Figure 2. The steady state kinetics of Rnt1p is defined by sustained product inhibition. (**A**) Comparison between the substrate and product. The predicted structure of Rnt1p substrate (TL) and its derived product (TL-PR) are shown in the form of a stem loop. The arrow indicates the position of the cleavage site. The cleaved strand is shown in gray. (**B**) Rnt1p products reduce enzymatic reactivity. The fluorescence profile of Rnt1p cleavage over time was determined as described in Figure 1C without product (−Product) or with the addition of equimolar amounts (0.8 μM) of Rnt1p product (+Product). (**C**) Rnt1p products reduce the rate of catalysis. The Michaelis–Menten kinetics of the initial rate of the reaction was determined in the absence (−Product) or the presence of 0.8 μM of the cleavage product (+Product). The data shown are the average of at least three independent experiments and the standard deviations are shown in the form of error bars. (**D**) Product removal enhances Rnt1p reactivity. The fluorescence profile of Rnt1p cleavage over time was determined as described in Figure 1C in the presence (+Xrn1p) or the absence (−Xrn1p) of the 5′-3′ exoribonuclease Xrn1p.

dicted, the addition of Xrn1p to the cleavage reaction significantly increased the steady state catalytic rate of Rnt1p without affecting the initial burst phase (Figure 2D). These data confirm the inhibitory effects of the cleavage products and underline their role in defining the steady state cleavage rate.

Rnt1p reactivity depends on substrate-specific cleavage product inhibition

Rnt1p RNA substrates are expressed at different levels and their turnover requirement varies based on the function of the mature RNA (8,18,11). For example, while efficient production of mature rRNA and snoRNAs may require rapid and constitutive cleavage by Rnt1p (8), selective degradation of mRNAs needs well controlled and in many cases conditional reactivity (9). To determine the impact of the substrate's natural structures on Rnt1p reactivity, we compared the reactivity of substrates with different levels of expression. The stem–loop structures found within the coding sequence of the glucose induced transcription repressor Mig2 (9) and the putative ATPase Yta6 (10,35) were chosen as model mRNA substrates, while the U5 snRNA (13) and U2 snRNA (12) processing signals were selected as representative non-coding RNA (Figure 3A). The different substrates were transcribed *in vitro* using T7 RNA polymerase and incubated with Rnt1p in the presence or

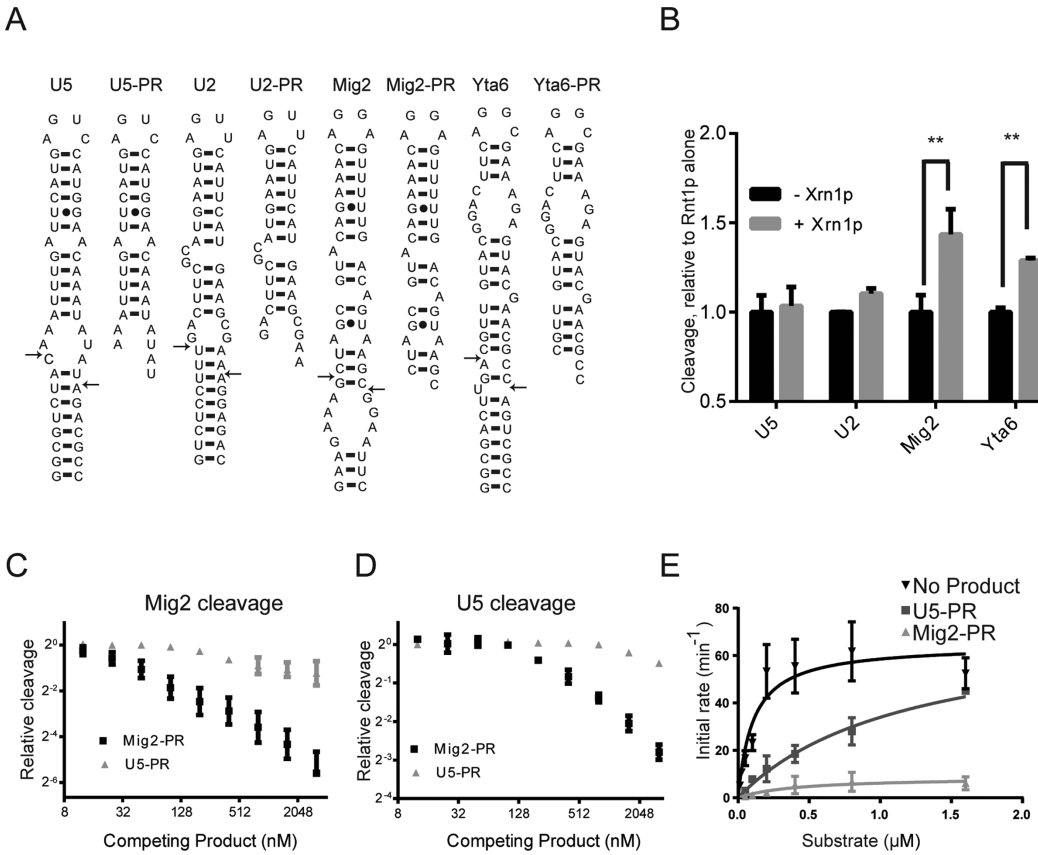

Figure 3. Product inhibition dictates the reactivity of natural mRNA degradation signals. (**A**) Schematic representation of four natural Rnt1p cleavage targets and their products. The substrates and products derived from two processing signals (U5 snRNA and U2 snRNA) and two degradation signals (Mig2 and Yta6 mRNAs) are shown. The arrows indicate the position of the established cleavage sites. (**B**) Product removal enhances the reactivity of mRNA-associated cleavage signals. An rnt1p cleavage assay was performed and the amount of cleaved substrate was determined in the presence (+Xrn1) or the absence (−Xrn1) of the exoribonuclease Xrn1p. Asterisks indicates significant difference between treatments (*P*-value <0.01). (**C**) Effects of Rnt1p cleavage products on the cleavage of Mig2 mRNA degradation signal. The cleavage of stem–loops derived from Mig2 mRNA was performed in the absence or the presence of increasing amounts of RNA products derived from Mig2 (Mig2–PR) or U5 (U5-PR). (**D**) Effects of Rnt1p cleavage products on the U5 snRNA processing. The cleavage of stem–loops derived from the U5 snRNA 3′ end was performed as described in (C) in the absence or presence of increasing amounts of RNA products derived from Mig2 (Mig2-PR) or U5 (U5-PR). (**E**) Kinetics of inhibition by U5 and Mig2 products. Michaelis–Menten curve of the TL substrate (Figure 2A) in the presence (U5PR or Mig2PR) or the absence (ND) of U5 or Mig2 products. The experiments shown are the average of three experiments and standard deviations are illustrated in the form of error bars.

the absence of the exoribonuclease Xrn1p to monitor the impact of product cleavage on the steady state reaction kinetics. Interestingly, the addition of Xrn1p did not alter the processing of the non-coding RNA U2 and U5, but it significantly enhanced the cleavage of the model mRNA substrates Mig2 and Yta6 (Figure 3B). To directly evaluate the effect of the cleavage products on Rnt1p reactivity, we monitored the impact of adding synthetic RNAs mimicking the products generated by the cleavage of the U5 snRNA (U5-PR) or the Mig2 mRNA (Mig2-PR) on the cleavage of U5 and Mig2. As indicated in Figure 3C and D, the processed Mig2 inhibited the cleavage of both Mig2 and U5, while U5 cleavage product did not. Accordingly, the addition of Mig2 products (but not U5) decreased the k_{cat} of the heterologous substrate TL (Figure 3E).

The turnover of Rnt1p substrates depends on the product release step

To examine the mechanism by which cleavage products inhibit Rnt1p reactivity, we compared the association (On) and dissociation (Off) rates of the inhibitory (Mig2-PR) and non-inhibitory (U5-PR) products, and their respective substrates, using plasmon resonance. As indicated in Figure 4A, the highly reactive U5 substrate had faster association and dissociation rates than, the moderately reactive substrate, Mig2. These results suggest that the Rnt1p–U5 catalytic complex has faster association and dissociation rates than the Rnt1p–Mig2 complex. Comparison between the association and dissociation kinetics of Mig2 and U5 products indicated that Mig2 products have a two-fold higher association rate (Figure 4C) and an 8-fold lower dissociation rate (Figure 4D). Comparison between the association and dissociation kinetics of the two substrates and their respective products indicated that while both the uncleaved U5 substrate and its product have similar affinity,

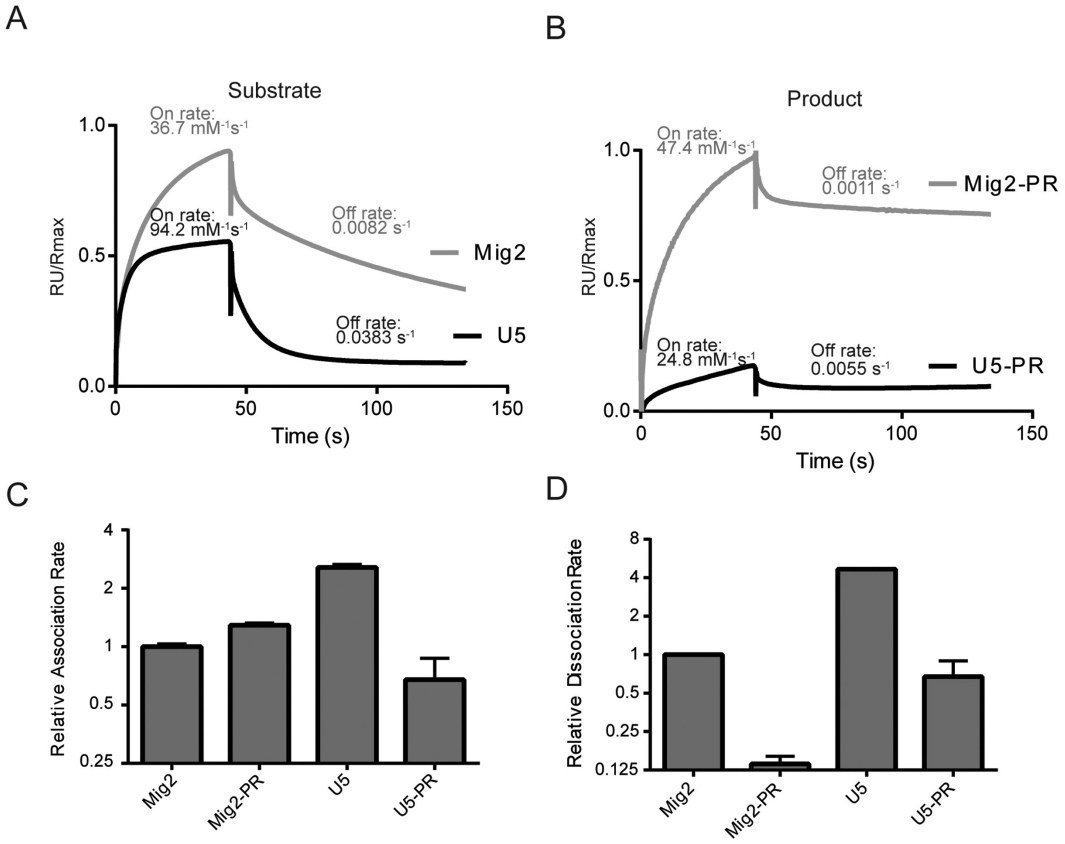

Figure 4. The product release step determines the reactivity of Rnt1p substrates. (**A**) Comparison between the association and dissociation kinetics of Mig2 (gray) and U5 (black) substrates. Rnt1p association and dissociation rates were determined using surface plasmon resonance in the presence of 10 mM Mg^{2+} and 150 mM KCl. The association and dissociation rates are indicated above each curve, as determined with a one site binding model using curves from concentrations of RNA from 50 to 1600 nM. (**B**) Comparison between the association and dissociation kinetics of Mig2 and U5 cleavage products. The association and dissociation rates were calculated as described in A and are indicated above each curve. (**C**) Comparison between the association rates of the substrate and products derived from Mig2 mRNA and U5 snRNA. (**D**) Comparison between the dissociation rates of the substrate and products derived from Mig2 mRNA and U5 snRNA. In (C) and (D), the association and dissociation kinetics obtained in A and B were calculated relative to that of Mig2 and are presented in the form of a bar graph with standard errors illustrated as error bars.

the Mig2 product associates ∼1.3-fold faster and dissociates ∼6.4-fold slower than its substrate (Figure 4C and D). These results indicate that the difference between U5 and Mig2 turnover is mostly the result of the low dissociation rate of the Mig2 cleavage product.

Identification of Rnt1p substrate reactivity determinants

To identify the specific sequence or structural features controlling Rnt1p substrate reactivity, we next compared the stem–loop structure of substrates with high (e.g. U5) versus low (e.g. Mig2) turnover rates. As indicated in Figure 5A, the Mig2 cleavage signal contains more paired nucleotides near the cleavage site and more asymmetrical bulges than that of U5. To evaluate the effect of the structure surrounding the cleavage site on Rnt1p reactivity, we created chimeric substrates composed of either the upper stem–loop of U5 fused to Mig2 cleavage site (U5–CMig2) or the upper stem–loop of Mig2 fused to U5 cleavage site (Mig2–CU5) and compared them to the original natural substrates. Interestingly, we found that the inclusion of the Mig2 cleavage site into the U5 structure (U5–CMig2) inhibited its cleavage by Rnt1p while the inclusion of the U5 cleavage site into the Mig2 substrate (Mig2-CU5) increased cleavage (Figure 5B). This indicates that the difference in processing between the U5 and Mig2 substrates is mainly caused by variations in the nature of the sequence surrounding the cleavage site. To evaluate the impact of the sequence surrounding Mig2 cleavage site on the capacity of the products to inhibit Rnt1p cleavage, we compared the effects of chimeric cleavage products that contain the Mig2 stem linked to the sequence upstream of the U5 cleavage site (Mig2–CU5–PR) to the unmodified Mig2 (Mig2–PR) and U5 (U5–PR) products on the cleavage of the Mig2 substrate. As shown in Figure 5C, the addition of the Mig2–PR inhibited Rnt1p reactivity while the addition of U5–PR or Mig2–CU5–PR had no effect. In addition, the replacement of the Mig2 sequence surrounding the cleavage site with that of U5 reduced the enzyme's affinity by drastically increasing the dissociation rates of the Mig2 product (Figure 5D). This indicates that the sequence surrounding Mig2 cleavage site specifically reduces the turnover rate by decreasing the rate of product release. We conclude that the reactivity of Rnt1p substrate reactivity is defined by determinants near the scissile bonds.

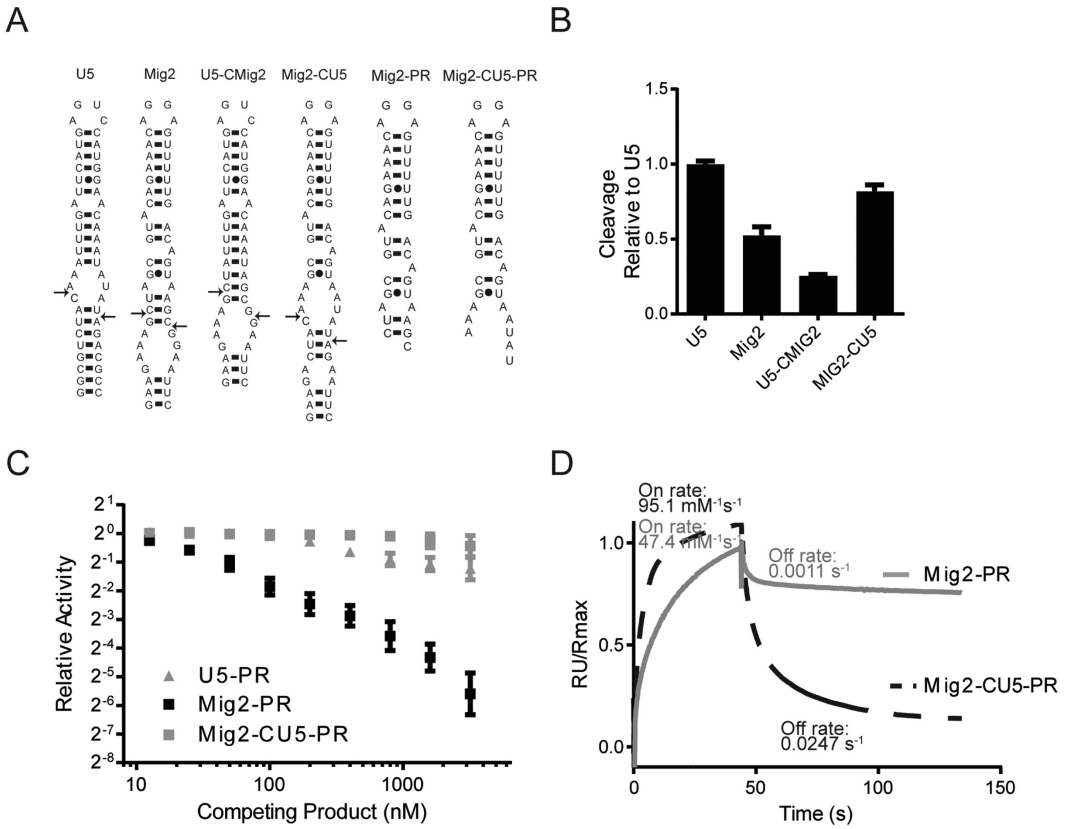

Figure 5. Identification of reactivity determinants near Rnt1p cleavage site. (**A**) Structure of chimeric U5 and Mig2 RNAs carrying mixed features of U5 and Mig2. U5 and Mig2 indicate the structure of natural U5 and Mig2 substrates. U5–CMig2 indicates a hybrid U5 substrate that carries the sequence of Mig2 surrounding cleavage site, while U5–CMig2–PR indicates the corresponding product after Rnt1p cleavage. Mig2–CU5 is a hybrid between Mig2 substrate and the sequence of U5 surrounding the cleavage site and Mig2–CU5–PR indicates the corresponding product after Rnt1p cleavage. (**B**) The structure surrounding the Mig2 cleavage site is sufficient for the inhibition of Rnt1p reactivity. The different substrates shown in (A) were assayed for cleavage by Rnt1p as described in Figure 3B and cleavage rates, relative to that obtained with the natural U5 substrate, are represented in the form of a bar graph. The data shown are the average of three independent experiments and the standard deviations are shown in the form of error bars. (**C**) The sequence surrounding the Mig2 cleavage site inhibits Rnt1p reactivity. The cleavage of Mig2 RNA was conducted with increasing amounts of oligonucleotides corresponding to Mig2, U5 or hybrid Mig2-CU5 products and the impact on cleavage for each product is reported in the graph. (**D**) The cleavage efficiency box determines the product binding and release rates. Comparison between the binding kinetics of the Mig2 product (Mig2–PR) and those of Mig2 product with the cleavage efficiency box of U5 (Mig2–CU5–PR). Association and dissociation rates were determined as in Figure 4 and are indicated above each graph.

The reactivity of Rnt1p substrates is defined by the base-pairing of the cleavage site

An obvious structural difference between Mig2 and U5 cleavage sites, which determines the nature of product termini, is the number of upstream paired nucleotides (Figure 6A). The termini of the U5 cleavage products are unpaired while those generated by Mig2 feature two terminal base-pairs (Figure 5A). To evaluate the impact of product termini base pairs on the inhibition of Rnt1p cleavage activity, we systematically mutated unpaired nucleotides in the U5 stem and tested the resulting substrates using Rnt1p cleavage assays in the presence or absence of Xrn1p. These experiments were designed to distinguish product-specific inhibition effects from other unrelated variations in substrate reactivity. As expected, only base pairs near the U5 cleavage site affected cleavage by Rnt1p in the presence of Xrn1p (Figure 6B). The introduction of the two base pairs immediately upstream of the cleavage site (substrates U5-4, U5-5 and U5-7) affected the cleavage by Rnt1p in the presence of Xrn1p (Figure 6B) and reduced the cleavage rate under multiple-turnover conditions without affecting cleavage activity under single-turnover conditions (Figure 6C). Mutations that created base pairs away from the cleavage site did not affect substrate cleavage by Rnt1p in the presence of Xrn1p (Figure 6B and C). This suggests that only base pairs located close to the cleavage site influence the steady state cleavage rate of Rnt1p.

Next we used our fluorescent assays to examine the role of base pairing near the Rnt1p cleavage site (Figure 1B). Fluorescent substrates with fully or partially complementary paired strands (Figure 7A) were assayed for Rnt1p-mediated cleavage. As shown in Figure 7B, introducing base pair mismatches upstream of the cleavage site disrupted the biphasic pattern observed in Rnt1p cleavage reaction and increased the steady-state turnover rate. We thus conclude that the reactivity of Rnt1p is depends on the number of base pairs upstream of the cleavage site.

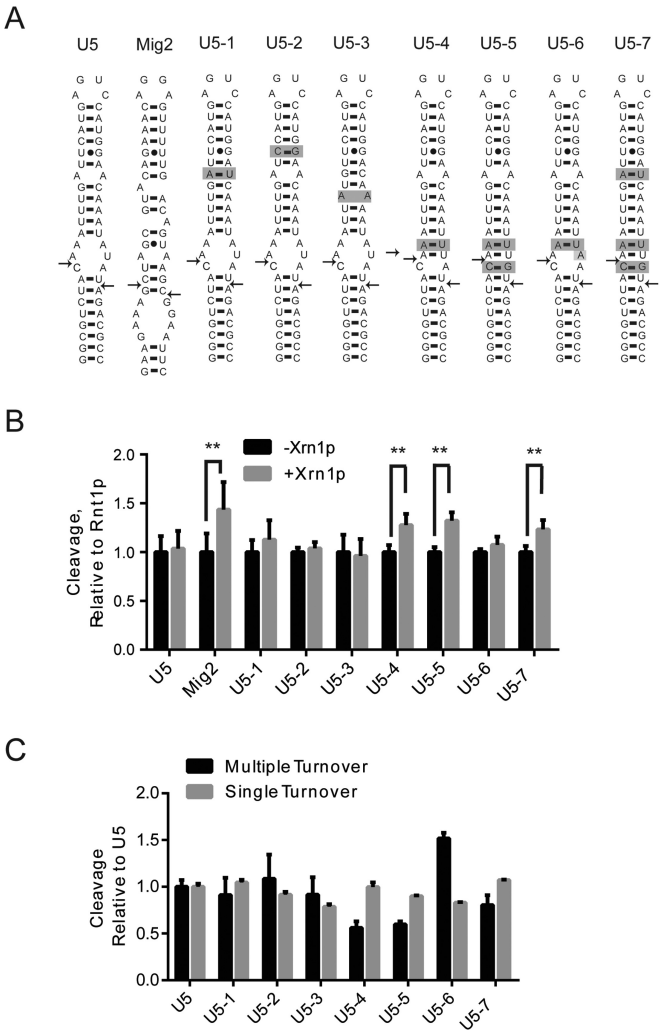

Figure 6. Rnt1p reactivity depends on the number of base-pairs upstream of the cleavage site. (**A**) Structures of U5 snRNA derivatives carrying mutations at unpaired sequences. U5 and Mig2 indicate the structure of U5 snRNA and Mig2 mRNA. U5-1, U5-2, U5-3, U5-4, U5-5, U5-6 and U5-7 indicate mutations in the U5 stem loops. The mutated sites are shaded and the cleavage sites are indicated with arrows. (**B**) Effect of base pairing on the product-dependent inhibition of RNA reactivity. The cleavage reaction of the each substrate was carried out as described in Figure 3B in the presence and in the absence of Xrn1p. The data are the average of at least three independent experiments. The asterisks indicate statistically significant differences (P-value < 0.01) in cleavage in comparison to the reaction in absence of Xrn1p. (**C**) Base pairing near the cleavage efficiency box reduces U5 turnover rate. The cleavage of the different versions of U5 substrates were carried as described in Figure 5B under both single and multiple turnover conditions and the different rates presented relative to that of U5.

DISCUSSION

This study describes the mechanism by which RNase III distinguishes between the substrates and the cleavage products and provides an explanation for how the enzyme controls expression of transcripts which the cell requires at different levels. Comparison between the substrates and the products of Rnt1p indicates that most of the enzyme's RNA-binding domains remain bound after cleavage, the exception being the RBM3 RNA-binding motif (Figure 1A). RBM3 binds to the substrate by interacting with 4 bp, two upstream and two downstream of the cleavage site, and only the 2 bp upstream of the cleavage site remain unaffected after cleavage. Disruption of these upstream base pairs increased the dissociation rate of the RNA, suggesting that dissociation from RBM3 triggers definitive product release (Figures 4 and 5). Consistently, increasing the number of base pairs upstream of the cleavage site increased the capacity of the products to inhibit Rnt1p presumably by stabilizing the interaction with RBM3. Together the data suggest that base-pairing of the product termini play an important role in determining the substrate turnover rate.

A previous study monitoring the intrinsic fluorescence of bacterial RNase III during catalysis indicated that the turnover rate is limited by a step subsequent to RNA hydrolysis, which was presumed to be either the product release step, or a change in the protein conformation after catalysis (26). Comparison between the structures of the catalytic and post-catalytic complexes of bacterial RNase III revealed that the RNA is distorted during cleavage and that its release from the catalytic site occurs in two steps which both require minor rearrangements in protein conformation (27,36,37). Consistently, our real time analysis of Rnt1p catalysis indicated a two-step process in which the product release is the rate-limiting step in the steady-state turnover rate (Figures 1 and 2). Indeed, comparison between the binding kinetics of different products shows that slow dissociation rate is an intrinsic feature of products that inhibit Rnt1p cleavage reaction (Figure 4). Product-dependent inhibition of RNase III enzymes likely arises from the high similarity between the products and the substrates; in most cases the cleavage products of this enzyme family retain affinity for the enzyme (2,23). This similarity is most clear in the case of Rnt1p, where most of protein interaction sites with the RNA are maintained in the product (Figure 1A). In bacterial RNase III, the dsRBD binds the RNA in the same region as the catalytic domain (27,36), while the dsRBD of Rnt1p binds to the tetraloop and its neighbouring stem structure (22). This unique mode of binding permits stable association with cleavage products and with short stems lacking the cleavage site (32). Therefore, while rate-limiting product release might be a general feature of RNase III, its impact is amplified in enzymes with special recognition mechanisms, like Rnt1p, where the RBM0 domain recognizes the tetraloop, and Dicer, where the PAZ domain specifically recognizes the two nucleotide 3′ overhang at the end of a hairpin structure (38).

In eukaryotes, RNA transcription and processing or degradation are well-integrated processes involving many factors. In yeast, it was shown that Rnt1p processes rRNA (39) and degrades a subset of its mRNA targets cotranscriptionally (40,41). After *in vivo* cleavage, Rnt1p products are exposed to downstream helicases and exoribonuclease that can eliminate free cleavage products (16,42). These observations suggested that the products would not control Rnt1p activity. Surprisingly we found *in vitro* that the product release, which is not affected by external factors, plays an important role in defining substrate reactivity. Product release limits the cleavage of conditionally degraded mRNA substrates like Mig2, which is regulated in a glucose-dependent manner (9), due to substrate-specific

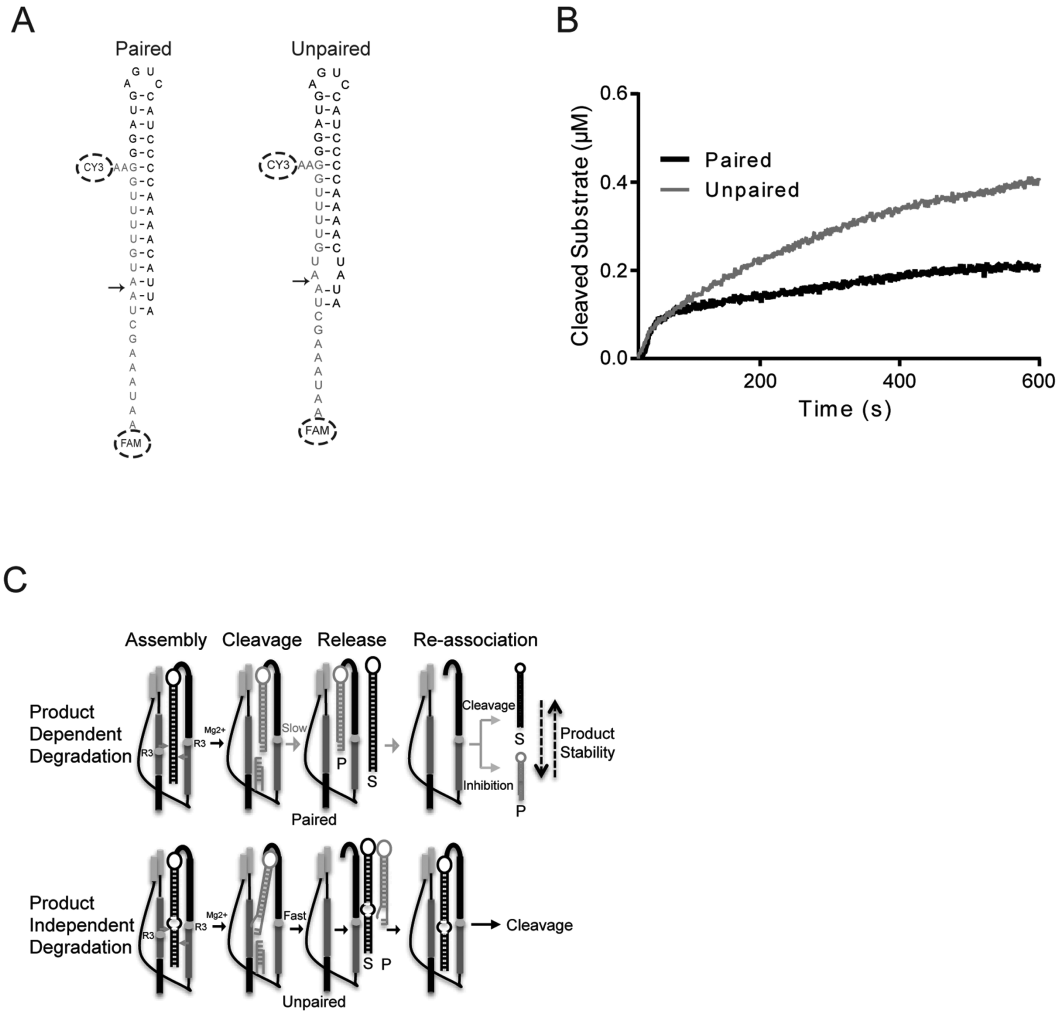

Figure 7. Pairing near the cleavage efficiency box modifies the initial rate of Rnt1p cleavage. (**A**) Structures of fluorescently labeled Rnt1p substrates with different pairing configurations near the cleavage site. (**B**) Cleavage profiles of substrates with different pairings at the cleavage site. The cleavage of fluorescent substrates was conducted as described in Figure 2D. (**C**) Mechanism of substrate determined enzymatic reactivity. The model illustrates how the structure of Rnt1p substrates influences the reactivity depending on the stability of the cleavage product. In this model, substrates with strong base-pairing near the cleavage site (e.g. mRNAs) undergo a product-dependent degradation reaction, where the reactivity is controlled by the rate of product release and association. On the other hand, substrates with unpaired nucleotides near the cleavage sites are cleaved irrespective of product levels and quickly released.

base pairing upstream of cleavage sites (Figures 5 and 7). Consistently, secondary structure comparison of hundreds of newly discovered Rnt1p substrates indicated that the sequence near the cleavage site is preferentially unpaired in non-coding RNAs that are cleaved efficiently by Rnt1p (10). Therefore, it appears that non-coding RNA substrates have evolved to avoid product inhibition.

Together the data presented in this study suggest a mechanism for two modes of RNA cleavage that depends on the nature of the substrate (Figure 7C). In the case of highly reactive RNA processing substrates, the assembly occurs readily and produces cleavage products with unpaired ends. This destabilizes the catalytic complex and triggers efficient product release, allowing the enzyme to be available for another round of catalysis. In this mode, the turnover rate reflects the catalytic rate and the efficient cleavage of an unlimited number of substrates can take place without the need to modify or degrade the products. In contrast, the degradation of less reactive regulated mRNA is product-dependent and has slower association and dissociation rates. In this mode of cleavage, the product release limits the turnover rate and the accumulating product can compete with the substrates in the absence of factors that modulate product stability or structure.

SUPPLEMENTARY DATA

Supplementary Data are available at NAR Online.

ACKNOWLEDGEMENTS

We thank Ute Kothe and members of the Abou Elela laboratory for critical reading of the manuscript.

FUNDING

Canadian Institutes of Health Research and the Canada Research Chair in RNA Biology and Cancer Genomics (to

S.A.). The funders had no role in study design, data collection and analysis, decision to publish, or preparation of the manuscript. Funding for open access charge: Canadian Institutes of Health Research.
Conflict of interest statement. None declared.

REFERENCES

1. Lamontagne,B., Larose,S., Boulanger,J. and Abou Elela,S. (2001) The RNase III family: a conserved structure and expanding functions in eukaryotic dsRNA metabolism. *Curr. Issues Mol. Biol.*, **3**, 71–78.
2. Nicholson,A.W. (2014) Ribonuclease III mechanisms of double-stranded RNA cleavage. *Wiley Interdiscip. Rev. RNA*, **5**, 31–48.
3. Bootcov,M.R., Bauskin,A.R., Valenzuela,S.M., Moore,A.G., Bansal,M., He,X.Y., Zhang,H.P., Donnellan,M., Mahler,S., Pryor,K. *et al.* (1997) MIC-1, a novel macrophage inhibitory cytokine, is a divergent member of the TGF-beta superfamily. *Proc. Natl. Acad. Sci. U.S.A.*, **94**, 11514–11519.
4. Ji,X. (2008) The mechanism of RNase III action: how dicer dices. *Curr. Top. Microbiol. Immunol.*, **320**, 99–116.
5. St Johnston,D., Brown,N.H., Gall,J.G. and Jantsch,M. (1992) A conserved double-stranded RNA-binding domain. *Proc. Natl. Acad. Sci. U.S.A.*, **89**, 10979–10983.
6. Robertson,H.D., Webster,R.E. and Zinder,N.D. (1968) Purification and properties of ribonuclease III from Escherichia coli. *J. Biol. Chem.*, **243**, 82–91.
7. Danin-Kreiselman,M., Lee,C.Y. and Chanfreau,G. (2003) RNAse III-mediated degradation of unspliced pre-mRNAs and lariat introns. *Mol. Cell*, **11**, 1279–1289.
8. Ghazal,G., Ge,D., Gervais-Bird,J., Gagnon,J. and Abou Elela,S. (2005) Genome-wide prediction and analysis of yeast RNase III-dependent snoRNA processing signals. *Mol. Cell. Biol.*, **25**, 2981–2994.
9. Ge,D., Lamontagne,B. and Abou Elela,S. (2005) RNase III-mediated silencing of a glucose-dependent repressor in yeast. *Curr. Biol.*, **15**, 140–145.
10. Gagnon,J., Lavoie,M., Catala,M., Malenfant,F. and Elela,S.A. (2015) Transcriptome wide annotation of eukaryotic RNase III reactivity and degradation signals. *PLoS Genet.*, **11**, e1005000.
11. Catala,M., Aksouh,L. and Abou Elela,S. (2012) RNA-dependent regulation of the cell wall stress response. *Nucleic Acids Res.*, **40**, 7507–7517.
12. Abou Elela,S. and Ares,M. Jr (1998) Depletion of yeast RNase III blocks correct U2 3' end formation and results in polyadenylated but functional U2 snRNA. *EMBO J.*, **17**, 3738–3746.
13. Chanfreau,G., Abou Elela,S., Ares,M. Jr and Guthrie,C. (1997) Alternative 3'-end processing of U5 snRNA by RNase III. *Genes Dev.*, **11**, 2741–2751.
14. Seipelt,R.L., Zheng,B., Asuru,A. and Rymond,B.C. (1999) U1 snRNA is cleaved by RNase III and processed through an Sm site-dependent pathway. *Nucleic Acids Res.*, **27**, 587–595.
15. Allmang,C., Kufel,J., Chanfreau,G., Mitchell,P., Petfalski,E. and Tollervey,D. (1999) Functions of the exosome in rRNA, snoRNA and snRNA synthesis. *EMBO J.*, **18**, 5399–5410.
16. Ghazal,G. and Elela,S.A. (2006) Characterization of the reactivity determinants of a novel hairpin substrate of yeast RNase III. *J. Mol. Biol.*, **363**, 332–344.
17. Abou Elela,S., Igel,H. and Ares,M. Jr (1996) RNase III cleaves eukaryotic preribosomal RNA at a U3 snoRNP-dependent site. *Cell*, **85**, 115–124.
18. Larose,S., Laterreur,N., Ghazal,G., Gagnon,J., Wellinger,R.J. and Elela,S.A. (2007) RNase III-dependent regulation of yeast telomerase. *J. Biol. Chem.*, **282**, 4373–4381.
19. Meaux,S., Lavoie,M., Gagnon,J., Abou Elela,S. and van Hoof,A. (2011) Reporter mRNAs cleaved by Rnt1p are exported and degraded in the cytoplasm. *Nucleic Acids Res.*, **39**, 9357–9367.
20. Lebars,I., Lamontagne,B., Yoshizawa,S., Aboul-Elela,S. and Fourmy,D. (2001) Solution structure of conserved AGNN tetraloops: insights into Rnt1p RNA processing. *EMBO J.*, **20**, 7250–7258.
21. Lavoie,M. and Abou Elela,S. (2008) Yeast ribonuclease III uses a network of multiple hydrogen bonds for RNA binding and cleavage. *Biochemistry (Mosc.)* **47**, 8514–8526.
22. Liang,Y.H., Lavoie,M., Comeau,M.A., Abou Elela,S. and Ji,X. (2014) Structure of a eukaryotic RNase III postcleavage complex reveals a double-ruler mechanism for substrate selection. *Mol. Cell*, **54**, 431–444.
23. Lamontagne,B. and Abou Elela,S. (2004) Evaluation of the RNA determinants for bacterial and yeast RNase III binding and cleavage. *J. Biol. Chem.*, **279**, 2231–2241.
24. Lamontagne,B., Ghazal,G., Lebars,I., Yoshizawa,S., Fourmy,D. and Abou Elela,S. (2003) Sequence dependence of substrate recognition and cleavage by yeast RNase III. *J. Mol. Biol.*, **327**, 985–1000.
25. Lamontagne,B., Tremblay,A. and Abou Elela,S. (2000) The N-terminal domain that distinguishes yeast from bacterial RNase III contains a dimerization signal required for efficient double-stranded RNA cleavage. *Mol. Cell. Biol.*, **20**, 1104–1115.
26. Campbell,F.E. Jr, Cassano,A.G., Anderson,V.E. and Harris,M.E. (2002) Pre-steady-state and stopped-flow fluorescence analysis of Escherichia coli ribonuclease III: insights into mechanism and conformational changes associated with binding and catalysis. *J. Mol. Biol.*, **317**, 21–40.
27. Blaszczyk,J., Gan,J., Tropea,J.E., Court,D.L., Waugh,D.S. and Ji,X. (2004) Noncatalytic assembly of ribonuclease III with double-stranded RNA. *Structure (Camb.)*, **12**, 457–466.
28. Blaszczyk,J., Tropea,J.E., Bubunenko,M., Routzahn,K.M., Waugh,D.S., Court,D.L. and Ji,X. (2001) Crystallographic and modeling studies of RNase III suggest a mechanism for double-stranded RNA cleavage. *Structure (Camb.)*, **9**, 1225–1236.
29. Lamontagne,B., Hannoush,R.N., Damha,M.J. and Abou Elela,S. (2004) Molecular requirements for duplex recognition and cleavage by eukaryotic RNase III: discovery of an RNA-dependent DNA cleavage activity of yeast Rnt1p. *J. Mol. Biol.*, **338**, 401–418.
30. Lamontagne,B. and Abou Elela,S. (2001) *Purification and Characterization of Saccharomyces cerevisiae Rnt1p Nuclease*. Academic Press, San Diego.
31. Pellegrini,O., Mathy,N., Condon,C. and Benard,L. (2008) In vitro assays of 5' to 3'-exoribonuclease activity. *Methods Enzymol.*, **448**, 167–183.
32. Lamontagne,B. and Abou Elela,S. (2007) Short RNA guides cleavage by eukaryotic RNase III. *PLoS One*, **2**, e472.
33. Lilley,D.M. (2009) The structure and folding of branched RNA analyzed by fluorescence resonance energy transfer. *Methods Enzymol.*, **469**, 159–187.
34. Larimer,F.W., Hsu,C.L., Maupin,M.K. and Stevens,A. (1992) Characterization of the XRN1 gene encoding a 5'–>3' exoribonuclease: sequence data and analysis of disparate protein and mRNA levels of gene-disrupted yeast cells. *Gene*, **120**, 51–57.
35. Schnall,R., Mannhaupt,G., Stucka,R., Tauer,R., Ehnle,S., Schwarzlose,C., Vetter,I. and Feldmann,H. (1994) Identification of a set of yeast genes coding for a novel family of putative ATPases with high similarity to constituents of the 26S protease complex. *Yeast*, **10**, 1141–1155.
36. Gan,J., Tropea,J.E., Austin,B.P., Court,D.L., Waugh,D.S. and Ji,X. (2006) Structural insight into the mechanism of double-stranded RNA processing by ribonuclease III. *Cell*, **124**, 355–366.
37. Gan,J., Shaw,G., Tropea,J.E., Waugh,D.S., Court,D.L. and Ji,X. (2008) A stepwise model for double-stranded RNA processing by ribonuclease III. *Mol. Microbiol.*, **67**, 143–154.
38. Bergeron,L. Jr, Perreault,J.P. and Abou Elela,S. (2010) Short RNA duplexes guide sequence-dependent cleavage by human Dicer. *RNA*, **16**, 2464–2473.
39. El Hage,A., Koper,M., Kufel,J. and Tollervey,D. (2008) Efficient termination of transcription by RNA polymerase I requires the 5' exonuclease Rat1 in yeast. *Genes Dev.*, **22**, 1069–1081.
40. Ghazal,G., Gagnon,J., Jacques,P.E., Landry,J.R., Robert,F. and Elela,S.A. (2009) Yeast RNase III triggers polyadenylation-independent transcription termination. *Mol. Cell*, **36**, 99–109.
41. Lavoie,M., Ge,D. and Abou Elela,S. (2012) Regulation of conditional gene expression by coupled transcription repression and RNA degradation. *Nucleic Acids Res.*, **40**, 871–883.
42. Ursic,D., Chinchilla,K., Finkel,J.S. and Culbertson,M.R. (2004) Multiple protein/protein and protein/RNA interactions suggest roles for yeast DNA/RNA helicase Sen1p in transcription, transcription-coupled DNA repair and RNA processing. *Nucleic Acids Res.*, **32**, 2441–2452.